

THIS REPORT HAS BEEN DELIMITED
AND CLEARED FOR PUBLIC RELEASE
UNDER DOD DIRECTIVE 5200.20 AND
NO RESTRICTIONS ARE IMPOSED UPON
ITS USE AND DISCLOSURE.

DISTRIBUTION STATEMENT A

APPROVED FOR PUBLIC RELEASE;
DISTRIBUTION UNLIMITED.

UNCLASSIFIED

AD 248 457

*Reproduced
by the*

ARMED SERVICES TECHNICAL INFORMATION AGENCY
ARLINGTON HALL STATION
ARLINGTON 12, VIRGINIA



UNCLASSIFIED

Best Available Copy

NOTICE: When government or other drawings, specifications or other data are used for any purpose other than in connection with a definitely related government procurement operation, the U. S. Government thereby incurs no responsibility, nor any obligation whatsoever; and the fact that the Government may have formulated, furnished, or in any way supplied the said drawings, specifications, or other data is not to be regarded by implication or otherwise as in any manner licensing the holder or any other person or corporation, or conveying any rights or permission to manufacture, use or sell any patented invention that may in any way be related thereto.

CATALOGUE
AS AD NO. 248

457

CARNEGIE INSTITUTE OF TECHNOLOGY

PITTSBURGH 13, PENNSYLVANIA

STRESS CORROSION CRACKING OF SINGLE CRYSTALS
OF SOME AUSTENITIC STAINLESS STEELS

1 October 1960

CONTRACT Nonr 760 (14) NR 036-029

169100

ASTIA
OCT 11 1960

Metallurgy Branch

OFFICE OF NAVAL RESEARCH

Washington 25, D. C.

61-1-5
NOX

Best Available Copy

STRESS CORROSION CRACKING OF SINGLE CRYSTALS
OF SOME AUSTENITIC STAINLESS STEELS

R. E. Reed^{*} B.S. M.S. Ph.D. and H. W. Paxton^{**} M.Sc. Ph.D.

-
- * Graduate Student, Carnegie Institute of Technology. Present address, Metallurgy Division, Oak Ridge National Laboratory, Oak Ridge, Tennessee. This paper is based on a thesis submitted as partial fulfillment of the requirements for the degree of Doctor of Philosophy.
- ** Firth Sterling Professor of Metallurgy, Carnegie Institute of Technology.

ABSTRACT

Detailed examination of the process of stress corrosion cracking in polycrystalline materials is handicapped by the inability to identify easily the crystallography of the process. Accordingly, the crack nucleation site, orientation of the crack plane, fracture time-stress relationship, fracture surface morphology, and corrosion product composition were studied during the stress corrosion cracking of austenitic stainless steel single crystals.

Fe-20Cr-20Ni, Fe-20Cr-12Ni, and commercial type 304 stainless steel single crystals were loaded in tension in boiling 42% MgCl₂ solution. The commercial type 304 stainless steel cracked or fractured in 4 to 17 hours, the Fe-20Cr-12Ni in 16-62 hours, and the Fe-20Cr-20Ni in 70-170 hours. The crack in all three alloys nucleated from elongated pits formed when portions of slip lines were attacked by the solution. The crack plane of the Fe-20Cr-20Ni specimens followed the (100) plane with the highest normal stress upon it. This is believed to be the first time that brittle cracks have been noted to follow a particular crystallographic plane in fcc material. Electron diffraction patterns made of the corrosion product from a Fe-20Cr-20Ni crack face showed that it may be a chromium-iron oxide. Colorimetric analysis of the corrosion solution showed an increase in nickel during the test.

The general crack plane in type 304 and Fe-20Cr-12Ni specimens was approximately normal to the tensile axis. Electron micrographs of the fracture surface on a type 304 specimen revealed possible crystallographic steps on a small scale.

It is proposed that the mechanism for this process probably consists of two stages: (1) a slow electrochemical crack initiation and re-initiation step and (2) a rapid mechanical fracture step.

Stress Corrosion Cracking of Single Crystals of Some
Austenitic Stainless Steels

R. E. Reed and H. W. Paxton

Introduction

The transgranular stress corrosion cracking of austenitic stainless steels has been extensively studied using polycrystalline material. The presence of grain boundaries and grains of differing orientations complicates the system under investigation. This makes it difficult to obtain information on nucleation sites, orientation of the crack plane, and the exact effect and magnitude of local stress. Consequently, the mechanism which accounts for the crack penetration is still not resolved.

This investigation makes use of some advantages inherent in single crystals. Single crystals enable the investigator to assign an orientation to the crack plane, locate the nucleation sites and to define the effect of stress more precisely and consequently to attempt to make a judgment as to the mechanism of crack penetration.

Previous work on stress corrosion cracking of single crystals has been reported for alpha brass, Cu_3Au , and a magnesium alloy. Wasserman⁽¹⁾ reported ammonia stress-cracking tests upon a 3/8 inch diameter single crystal of Cu-36% Zn. This fractured after 1.5% elongation in a moist ammonia atmosphere. The fractures were normal to the tensile axis and followed no definite crystal lattice plane.

The cracks originated where the major axes of the glide ellipses intersected the specimen surface.

Edmunds⁽²⁾, using very inhomogeneous single crystals (coring was clearly evident), produced failure in wet ammonia atmosphere. He noted the cracks were normal to the tensile axis.

Tragert⁽³⁾, using well-homogenized single crystals of dilute Cu-P alloys in ammonia, found that the crack plane showed no crystallographic dependence. He reported that the surface traces of slip planes were preferentially attacked.

Skorcheletti and Titova⁽⁴⁾ showed that the time to failure of alpha brass single crystals in ammonia atmospheres at constant stress is dependent upon the relative orientation of the slip plane to the tensile axis of the specimen. No details or orientation were given for the crack plane.

Edeleanu⁽⁵⁾ recently made some visual observations on stressed alpha brass single crystals in an ammonia atmosphere. He watched the progress of cracking at a magnification of 700X. The cracks seemed to move in "bursts", being stopped at slip traces and then, after some time interval, propagating rapidly to another slip trace. The general direction of the crack was at right angles to the applied stress. However, it sometimes tended to follow roughly the trace of a possible slip plane.

Bakish and Robertson⁽⁶⁾ in a paper on the corrosion of Cu_3Au in ferric chloride made some interesting observations on active sites of corrosion. They found that the preferential corrosion of Cu apparently followed dislocation patterns. Later⁽⁷⁾, they used this system for

stress corrosion cracking studies. From their results, obtained upon cracking single crystals of Cu_3Au in ferric chloride, they concluded that plastic strain is a prerequisite for rapid fracture. Most of the cracks originated in slip clusters. The plane of initial crack growth was normal to the axis of tension and unrelated to any particular crystallographic plane.

Maller and Metzger⁽⁸⁾ performed some stress corrosion cracking experiments on AZ 61 x magnesium alloy single crystals stressed in salt-chromate solutions. The experiments showed that plastic deformation was necessary to promote stress corrosion cracking in reasonable times. Metzger⁽⁹⁾ later reported that the cracks in this system were crystallographic and followed (1010), (1101), and (0001) planes depending upon the orientation of the specimen. Priest, Beck and Fontana⁽¹⁰⁾ found the crack plane to be the basal plane in large grained samples of the same alloy.

No reported work has been done using single crystals of stainless steel. However, two papers have been presented reporting experiments on the stress corrosion cracking of large-grained austenitic stainless steel. Logan and Sherman⁽¹¹⁾ did some work on large-grained 18-8 stainless steel in chloride solution. They used specimens with a rectangular cross-section and examined grains on an edge so that the trace of a crack plane could be followed on two planes at right angles. They concluded that the crack plane was apparently crystallographically random and approximately normal to the tensile axis.

Leu and Nello⁽¹²⁾ examined types 304, 317, 347, and 310 austenitic stainless steels which were stress corrosion cracked in boiling 42%

MgCl₂. The large grain size was obtained by recrystallization and grain growth at 1250°C. They concluded that the cracks formed were all in a plane perpendicular to the orientation of the highest tensile stresses and showed no relation whatsoever to the lattice structure of the metal. Also they noted that corrosive attack on the slip bands resulted in pitting. Cracks then formed having their origin at these pits.

A large amount of experimentation has been done on the stress corrosion cracking of polycrystalline austenitic stainless steels. The effect of stress upon the time to fracture in polycrystalline 18-8 material in boiling 42% MgCl₂ solution is generally reported in the form of figure 1.⁽¹³⁾ A threshold stress for stress corrosion is difficult to measure. For reasonable experimental times, say of order 10,000 minutes, reported threshold stresses vary from zero applied stress to the yield stress.

The effect of nickel composition upon the time to failure in boiling 42% MgCl₂ has been reported by Edeleanu⁽¹⁴⁾ in the form shown by figure 2. These data indicate that 18% is needed in a Fe-18% Cr alloy to prevent stress corrosion failure in 100 hours. Copson⁽¹⁵⁾ has reported that roughly 42% Ni is needed to prevent failure in 100 hours. This is typical of the scatter found in the stress corrosion literature.

Experimental Techniques

The single crystals used in this study were grown from the melt. For this reason, the bulk of this study was completed using an Fe-20 Cr-20 Ni alloy since this composition results in an entirely austenitic alloy in the as cast condition. Later attempts to produce single crystals from a Fe-20 Cr-12 Ni alloy and a commercial 304 stainless steel were also successful. This is surprising since both of these alloys contain substantial amounts of secondary delta ferrite after solidification from the melt, and according to the only available phase diagram⁽³²⁾ should in fact show primary delta on cooling.

The starting material consisted of two vacuum-melted Fe-Cr-Ni laboratory alloys and a commercial type 304 stainless steel. The compositions of these alloys are listed in Table I.

TABLE I

Chemical Analyses for Starting Material

| <u>Type Material</u> | <u>Cr</u> | <u>Analysis Ni</u> | <u>(Weight Per Cent)</u> | |
|---|-----------|------------------------|--------------------------|----------|
| | | | <u>C</u> | <u>N</u> |
| Vac. melted Fe-20Cr-20Ni 3/4" sq. bar | 19.73 | 20.31 | .0012 | .0080 |
| Vac. melted Fe-20Cr-12Ni 5/8" sq. bar | 19.82 | 12.14 | .0014 | .0048 |
| Commercial 304 | 18.36 | 9.45 | .036 | .032 |

The method for growing the single crystals from the melt essentially consisted of pulling a horizontal boat of molten metal through a temperature gradient which spanned the liquidus-solidus range of temperature.

The experimental techniques necessary to accomplish this have been described elsewhere by Leggett, Reed and Paxton⁽¹⁶⁾. This resulted in single crystals which contained a substructure which had a maximum misorientation of the order of 1°. Chromium oxide inclusions were also present.

In the case of the Fe-20Cr-12Ni and commercial 304 alloys, the as-grown ingot was annealed at 1200°C for 84 hours in a dry hydrogen atmosphere in order to eliminate the delta ferrite. The as-cast ingots of Fe-20Cr-20Ni, or the annealed ingots of the other alloys, were then mounted in Wood's metal and sliced lengthwise into slabs 100 mils thick. This was done using a slitting saw, 20 mils thick, which was mounted on a milling machine. Four slices were obtained from each ingot.

These slabs were then carefully machined into tensile specimens by milling a reduced gage length and drilling a pin hole at each end.

The specimens were chemically polished until about 20 mils of material were removed. The solution used was equal parts of hydrochloric acid, 30% hydrogen peroxide, and water. The speed of polish was controlled by varying the hydrogen peroxide content.

After the chemical polish, the surfaces of the reduced gage were polished lightly on #600 waterproof silicon carbide paper under water. The specimens were then electropolished until all scratches were entirely removed. The solution used for this was 7 parts 65% perchloric acid and 10 parts glacial acetic acid. The current density was about 0.4 amperes per square centimeter. The chromium oxide inclusions were preferentially attacked by the electropolish leaving pits.

An annealing treatment of 1200°C for 12 hours in dry hydrogen followed by a furnace cool was then used. After this, the specimens were electropolished for one minute. This was the final step before stress corrosion testing. At this stage, the specimens were about 2 1/2 inches long, 1/2 inch wide, and 60-80 mils thick with a reduced gage length 1 inch long and 140-180 mils wide. The holes in each end were 125 mils in diameter.

All of the specimens were loaded in tension in boiling aqueous 42% MgCl₂ solution at 154°C. The apparatus used for this purpose is shown schematically in figure 3. All of the assembly that held the specimen was made of titanium. Potential measurements between the titanium grips and Fe-20Cr-20Ni specimens showed the specimen to be anodic to the titanium.

Usually one specimen from each single crystal ingot was pre-strained in order to determine the critical resolved shear stress for that ingot. This was done on an Instron TTCL Tensile Machine using silicone oil at 154°C. The remainder of the specimens from the ingot were strained in the MgCl₂ solution at 154°C.

Corrosion was generally continued until cracks were readily visible to the eye. At this stage, the specimen was removed. The angles that the crack made with a common edge, as measured on two surfaces at right angles determined the pole of the crack plane⁽¹⁷⁾.

The electron microscopy was done using the oxide replica technique developed by Nielsen and Mahla⁽¹⁸⁾. The profile of the fracture surfaces

was also examined by nickel plating the crack surface and sectioning the composite sample.

Results

The Fe-20Cr-20Ni single crystals exhibited a yield point phenomenon. A typical load-elongation curve showed a marked upper yield point and then an unusually long Luder's extension region which generally was 6-10% strain. Usually one primary (111) slip plane was active. Little, if any, cross slip was observed. The critical resolved shear stress based on the value of the upper yield load was determined to be about 4000 psi at 154°C.

It was possible to obtain stress corrosion cracking in single crystals of all the alloys tested. It was found necessary to plastically deform all Fe-20Cr-20Ni specimens in order to obtain stress corrosion cracking in reasonable times. At stresses below the upper yield stress cracking did not occur in 800 hours. Stresses at or slightly above the upper yield stress would cause cracking or fracture in 70 to 170 hours. The cracks in all specimens where a check was possible started where the majority of slip was by edge components of dislocations. The effect of stress upon the time to failure was determined for the Fe-20Cr-20Ni alloy. After plastic deformation, the time to failure seemed to be insensitive to the stress level used during the corrosion test. Test stresses, ranging from 1.0 to 2.5 times the upper yield stresses for the Fe-20Cr-20Ni single crystals, exhibited no systematic effect upon the times to failure which again varied from 70 to 170 hours.

Some visual observations were made at 150x magnification during stress corrosion cracking. It was noted here that suddenly increasing the tensile stress did not result in any immediate crack propagation. Instead, the crack widened with evidence of considerable plastic deformation at the crack tip.

Fe-20Cr-12Ni and commercial 304 single crystals were tested at a nominal stress of 10,000 psi which corresponded to a stress above the upper yield stress of Fe-20Cr-20Ni. Both alloys exhibited plastic deformation at this stress which was similar to the Luder's extension shown by the Fe-20Cr-20Ni alloy. The times to failure for all of the alloys exposed to boiling 42% MgCl₂ at similar stresses are listed in Table II.

TABLE II

Time to Failure for Fe-20Cr-20Ni, Fe-20Cr-12Ni, and Commercial 304 Crystals Tested at Stresses Slightly Above the Upper Yield Stress in Boiling 42% MgCl₂.

| <u>Composition</u> | <u>Time to Failure</u> |
|--------------------|------------------------|
| Fe-20Cr-20Ni | 70-170 hours |
| Fe-20Cr-12Ni | 16-62 hours |
| Commercial 304 | 4-17 hours |

There were two nucleating sites for stress corrosion cracks in all of the single crystals. One such site was the pits which were present on the surface of the specimen prior to testing due to the preferential attack on the chromium oxide inclusions by the electropolishing action. This type of site is shown in figure 4.

The other common site was an attacked slip plane trace which became an elongated pit. Figure 5 illustrates this type of site.

In some instances a specimen contained recrystallized areas which formed during the final annealing treatment. During subsequent stress corrosion testing, the grain boundaries present acted as nucleating sites for stress corrosion cracks (Figure 6). Upon examination at higher magnifications, it was observed that these cracks actually nucleated from attacked slip lines near the grain boundary (Figure 7).

During the stress corrosion testing of the Fe-20Cr-20Ni alloy, it was observed that the specimens strained in the $MgCl_2$ solution developed many more cracks than those specimens that were prestrained. However, the times to failure did not seem to be appreciably different.

Figure 6 also suggests strongly the crystallographic nature of the crack plane for the Fe-20Cr-20Ni alloy. Another observation made about some cracks in recrystallized regions is that the crack plane changed direction when crossing a twin boundary (Figure 8). A typical stress corrosion crack as seen in a single crystal of Fe-20Cr-20Ni is shown in Figure 9 which is a composite of two photomicrographs. The large angle made with the tensile axis is especially obvious here.

The Fe-20Cr-20Ni alloy was quite different from the Fe-20Cr-12Ni and commercial 304 alloys with regard to the crystallographic orientation of the crack plane. The plane of the stress corrosion cracks in single crystals of Fe-20Cr-20Ni was the (100) plane which had the greatest normal stress upon it. The data illustrating this point are presented in Figure 10. Here the crack plane poles and the tensile axes for

the specimens tested are plotted on the unit triangle. The numbers refer to an ingot number which usually represents four specimens. It is evident that the crack plane poles can be identified within experimental error as (001) type poles in all cases.

The Fe-20Cr-12Ni and commercial 304 single crystals developed cracks which were roughly normal to the tensile axis and unrelated to any crystallographic plane over long distances. This is best shown by Figure 11.

Examination of the crack surfaces also revealed marked differences in surface morphologies. The structure observed on the Fe-20Cr-20Ni fracture surfaces supported the result that these surfaces are predominantly (100) over their entire area. First, it was noted that slip plane traces visible on these surfaces intersected at right angles. In the fcc lattice it can be shown that the (111) slip plane traces intersect at right angles only if viewed on a (100) face.

Second, a "cubic block structure" was observed on these surfaces which is typical of (100) type surfaces. This is illustrated by figure 12. Figure 13 shows other features observed on the Fe-20Cr-20Ni crack surfaces. Here, ledges on the surface are noted to have step-wise patterns on their leading edges.

The crack surfaces of the commercial 304 single crystals did not exhibit any structure which would associate the general crack surface with a particular crystallographic plane. Instead, it appeared to be made up of small facets, possibly crystallographic, which are less than a micron in size. This structure is similar to that reported for a

polycrystalline type 316 stainless steel by Nielsen⁽¹⁹⁾. Figure 14 shows the surface features on a crack plane of commercial 304.

The profile of the crack surfaces, as examined by nickel plating and sectioning, exhibited a similar difference in morphology between the Fe-20Cr-20Ni alloy and the Fe-20Cr-12Ni and commercial 304 alloys. Figure 15 presents a fracture surface profile of a Fe-20Cr-20Ni single crystal. The nickel plate is at the top of the photomicrograph. Corrosion product is in evidence at the corners of the jogs and where side cracks nucleate.

Similar treatment of crack surfaces on Fe-20Cr-12Ni and commercial 304 did not show sharp crystallographic features on the same scale as found in the Fe-20Cr-20Ni. Resolution of facets of about 0.1 micron is not possible by this technique.

The reasons for the variation of behavior with composition are not clear to the authors. Various proposals have been made in the past, but none of them are definitive and it is apparent that careful measurements are necessary to identify the cause of the composition dependence.

Attempts to identify the insoluble green corrosion product on the fracture surfaces of Fe-20Cr-20Ni single crystals by electron diffraction patterns were not completely successful but results indicate the presence of a mixed chromium-iron oxide. Chemical analyses on the test solutions used in the stress corrosion cracking of Fe-20Cr-20Ni single crystals show the solution increased in nickel content but little or no iron or chromium went into solution.

DISCUSSION

There are several proposed mechanisms for transgranular stress corrosion cracking of austenitic stainless steels. Essentially, these mechanisms divide into two main groups.

One group holds that crack penetration is entirely electrochemical in nature with mechanical assistance due to the applied stress. This "mechanical assistance" may take the form of film rupture as proposed by Logan (20); it may be the formation of strained material at the tip of the crack as suggested by Hoar and Hines (21); it may produce a strain-induced transformation at the tip of the crack as advanced by Edleanu(22); or it could cause accelerated anodic dissolution at the tip of the crack due to the continual arrival of dislocations at the surface as proposed by Hoar and West (23). All of these "mechanical assists" create an anodic region at the tip of the crack which is then continually dissolved by an electrochemical process which results in crack penetration.

The other group contends that a crack penetrates by a repetitive process of electrochemical nucleation of a crack followed by a mechanical fracture crack propagation. Keating (24) first proposed this type of mechanism to account for the rapid crack penetration rates noted in stress corrosion. He offered no detailed mechanism. Harwood (25) suggested that electrochemical attack created a "notch" which then deformed at the tip and developed crack nuclei in this area. These nuclei would then propagate if the conditions for brittle crack propagation existed in this system.

A crack nucleus can propagate if conditions exist such that either the local yield stress for the material is raised above the stress necessary for brittle fracture or the brittle fracture stress for the material is somehow lowered below the yield stress. Recently, detailed mechanisms have been advanced that could accomplish one or the other of these conditions.

Forty (26) has suggested a mechanism for the stress corrosion cracking of alpha brass single crystals. He proposes that cracks nucleate from elliptical voids created on slip planes by a vacancy condensation process and propagate through the material due to the local raising of the yield stress by short range order at the strain rates involved. It is not easy to reconcile this nucleation step proposed with the observations of Wasserman⁽¹⁾ and the present authors that cracks nucleate on the major axis of the glide ellipse.

Paxton, Reed, and Leggett (27) proposed a similar type of reasoning for austenitic stainless steel. Here, a crack propagating at high rates could conceivably do so due to the local raising of the yield stress because of the presence of stacking faults. This is possible if the dislocations are widely dissociated because of a low stacking fault energy, thus increasing the stress required to force one through another, especially at high strain rates where little help is expected from thermal activation. However, recent experiments performed by Meyrick (28) on the fracture characteristics of stainless steel at quite high strain rates indicate that this is insufficient to explain crack propagation.

Swann and Nutting (29) have recently suggested that there may be a chemical interaction between the solute element and the stacking fault. Their results show that there is an uneven distribution of solute in deformed alloys of low stacking fault energy and the active slip planes become enriched in solute.

Other investigators have considered mechanisms whereby the brittle fracture stress necessary for crack propagation is decreased. Uhiig (30) has suggested that selective adsorption of ions which lower the surface energy of the crack nucleus (and thus favor crack propagation) operates conjointly with electrochemical action along paths where defects predominate and where compositional gradients exist. This results in discontinuous crack penetration. Coleman, Weinstein, and Kostoker (31) attempted to measure a surface energy reduction for stress corrosion cracks in 18-8 exposed to boiling 42% $MgCl_2$. They estimated a reduced surface energy of 100-200 $ergs/cm^2$ for these cracks versus about 1500 $ergs/cm^2$ which is a normal surface energy for this material. They also propose a crack propagation step due to adsorption lowering the surface energy of the crack nucleus.

Some common observations noted in stress corrosion cracking of stainless steels are listed below. These would have to be explained by any proposed mechanism for this process.

- (a) The chloride ion is particularly effective in causing stress corrosion cracking of austenitic stainless steel.
- (b) Cathodic protection stops crack penetration.

(c) Pure metals in general and ferritic (bcc) stainless steels in general apparently do not exhibit transgranular stress corrosion cracking.

(d) Plastic deformation seems to be necessary for cracking in reasonable times.

Now the necessity for plastic deformation and the presence of a solute in an fcc lattice may mean that solute segregation at dislocation structures may play a role in stress corrosion. Stacking faults may be the "dislocation structure" since bcc stainless steels are not susceptible. Since nickel was preferentially dissolved in this investigation, then it is conceivable that nickel segregates to stacking faults causing compositional gradients in the material. That this can happen in copper alloys was shown by Swann and Nutting(29).

Therefore, an electrochemical action could take place along the active slip planes due to this solute segregation. This could possibly directly create a crack nucleus or the deformation resulting from the formation of a sharp "chemical notch" could cause the creation of a crack nucleus.

How this crack propagates is not quite clear. It is not yet certain whether the local yield stress is increased due to the presence of short range order or stacking faults at the strain rates involved or whether the necessary brittle fracture stress is lowered possibly because of surface energy reduction due to adsorption.

The experimental results of this investigation favor the electrochemical-mechanical mechanism. The observed fracture surface morphologies

would not be expected if an electrochemical mechanism were operative. Also the crack penetration rates observed, such as roughly 1mm/hr for commercial 304, 0.1 mm/hr for Fe-20Cr-12Ni, and 0.5 mm/hr for Fe-20Cr-20Ni, cannot be reasonably explained by an anodic dissolution process if the expected polarization effects are considered.

CONCLUSIONS

- (1) It is possible to obtain stress corrosion cracking in commercial 304, Fe-20Cr-12Ni, and Fe-20Cr-20Ni single crystals loaded in tension in boiling 42% MgCl₂.
- (2) Test stresses, ranging from 1.0 to 2.5 times the upper yield stresses for the Fe-20Cr-20Ni single crystals, exhibited no systematic effect upon the times to fracture.
- (3) Plastic deformation is necessary to crack Fe-20Cr-20Ni single crystals in reasonable times.
- (4) Cracks initiate primarily at elongated pits resulting from slip line attack in austenitic stainless steel single crystals.
- (5) The general crack plane of the commercial 304 and Fe-20Cr-12Ni single crystals is approximately normal to the tensile axis and is not obviously associated with a crystallographic plane.
- (6) The crack plane of the Fe-20Cr-20Ni single crystals is the (100) plane with the greatest normal stress. The reasons for the difference between this composition and the others are not clear.
- (7) It is suggested that the results of this investigation more closely fit a mechanism of (a) a slow electrochemical crack initiation and (b) a rapid mechanical fracture step.

ACKNOWLEDGMENTS

The authors are grateful to the Office of Naval Research and Firth-Sterling, Inc., for financial support. Allegheny-Ludlum Steel Corporation and the United States Steel Corporation very kindly supplied materials and chemical analyses. A special expression of appreciation should be given to Dr. N. A. Nielsen of E. I. DuPont de Nemours and Co., Inc., for the electron microscopy performed and to Dr. Glyn Meyrick of Carnegie Institute of Technology for much helpful assistance.

REFERENCES

- (1) G. Wassermann, Zeitschrift für Metallkunde 34 (1942), p. 297.
- (2) G. Edmunds, Symposium on the Stress Corrosion Cracking of Metals, ASTM-AIME (1944), p. 67.
- (3) W. E. Tragert, Master's Thesis, Yale University (1951).
- (4) V. V. Skorchelletti and V. A. Titova, Journal of Applied Chemistry (U.S.S.R.) 26 (1953), p. 41.
- (5) C. Edeleanu, Physical Metallurgy of Stress Corrosion Fracture, T. N. Rhodin, ed., Interscience Publications (1959), p. 79.
- (6) R. Bakish and W. D. Robertson, Acta Met. 3 (1955), p. 513.
- (7) R. Bakish and W. D. Robertson, Acta Met. 4 (1956), p. 342.
- (8) F. Meller and M. Metzger, U. S. National Advisory Committee on Aeronautics Technical Note (1957), No. 4019, 22 pages.
- (9) M. Metzger, Physical Metallurgy of Stress Corrosion Fracture, T. N. Rhodin, ed., Interscience Publishers, New York (1959), discussion to C. Edeleanu's paper, p. 94.
- (10) D. K. Priest, F. H. Beck, and M. G. Fontana, Transactions ASM 47 (1955), p. 486.
- (11) H. L. Logan and R. J. Sherman, Welding Journal 35 (1956), p. 389s.
- (12) K. Leu and J. Helle, Corrosion 14 (1958), p. 249t.
- (13) T. P. Hoar and J. G. Hines, Stress Corrosion Cracking and Embrittlement, W. D. Robertson, ed., John Wiley and Sons, New York (1956), p. 107.
- (14) C. Edeleanu, Stress Corrosion Cracking and Embrittlement, W. D. Robertson, ed., John Wiley and Sons, New York (1956), p. 126.
- (15) H. R. Copson, Physical Metallurgy of Stress Corrosion Fracture, T. N. Rhodin, ed., Interscience Publishers, New York (1959), p. 247.
- (16) R. D. Leggett, R. E. Reed and H. W. Paxton, Trans. AIME 215 (1959), p. 679.
- (17) C. S. Barrett, Structure of Metals, McGraw-Hill Book Company, New York (1952), p. 40.

- (18) N. A. Nielsen and E. M. Mahla, Journal of Applied Physics, 19 (1948), p. 379.
- (19) N. A. Nielsen, Physical Metallurgy of Stress Corrosion Fracture, T. N. Rhodin, ed., Interscience Publishers, New York (1959), p.121.
- (20) H. L. Logan, Journal of Research, National Bureau of Standards 48 (1952), p. 99.
- (21) T. P. Hoar and J. G. Hines, Journal of the Iron and Steel Institute 182 (1956), p. 124.
- (22) C. Edeleanu, Journal of the Iron and Steel Institute 173 (1953), p. 140.
- (23) T. P. Hoar and J. M. West, Nature 181 (1958), p. 835
- (24) F. H. Keating, Symposium on Internal Stresses in Metals and Alloys, Institute of Metals (1948), p. 329.
- (25) J. J. Harwood, Stress Corrosion Cracking and Embrittlement, W. D. Robertson, ed., John Wiley and Sons, New York (1956), p.1.
- (26) A. J. Forty, Physical Metallurgy of Stress Corrosion Fracture, T. N. Rhodin, ed., Interscience Publishers, New York (1959), p.99.
- (27) H. W. Paxton, R. E. Reed, and R. D. Leggett, Physical Metallurgy of Stress Corrosion Fracture, T. N. Rhodin, ed., Interscience Publishers, New York (1959) p. 181.
- (28) G. Meyrick, unpublished work done at Metals Research Laboratory, Carnegie Institute of Technology, Pittsburgh 13, Pennsylvania, 1959-1960.
- (29) P. R. Swann and J. Nutting, Structure and Properties of Thin Films, John Wiley and Sons, New York (1959), p. 196.
- (30) H. H. Uhlig, Physical Metallurgy of Stress Corrosion Fracture, T. N. Rhodin, ed., Interscience Publishers, New York (1959), p.1.
- (31) E. G. Coleman, D. Weinstein, and W. Rostoker, ONI Technical Report ARF 2152-10, Armour Research Foundation of Illinois Institute of Technology, February, 1960.
- (32) R. H. Aborn and E. C. Bain, Metals Handbook, American Society for Metals, Cleveland, Ohio, (1948).

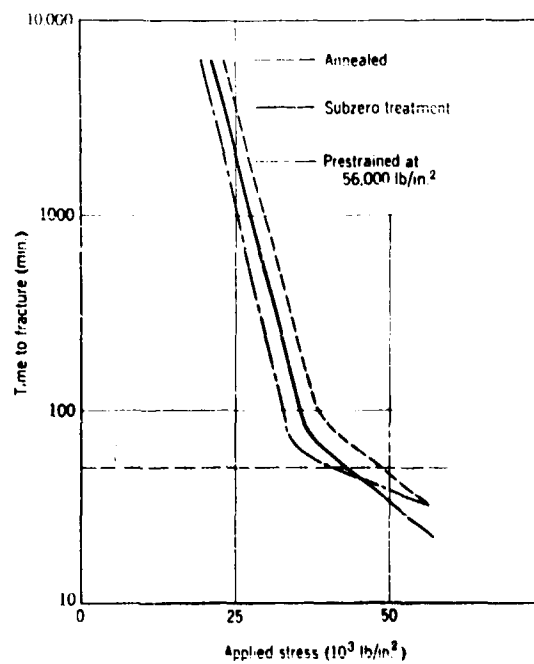


Figure 1. Variation of Time to Fracture with Applied Stress. Steel 18-8: fully softened; prestrained at 56,000 psi; and refrigerated at -184°C for 1/2 hour. Tested at $152-153^{\circ}\text{C}$ (13).

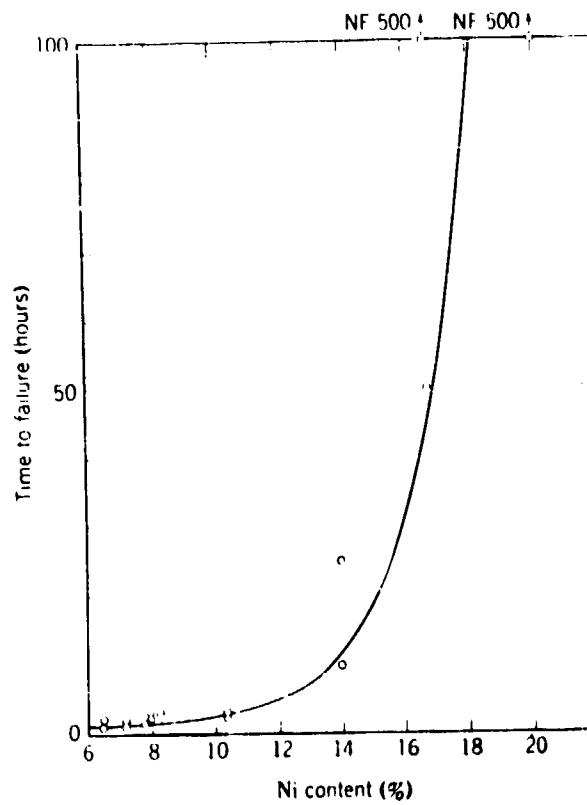


Figure 2. Time to failure of steels with 17-18% Cr and with various nickel contents. Tests were conducted in boiling 42% $MgCl_2$ on 0.1685 inch tensile specimens stressed to 40,000 psi (Nominal)(14).

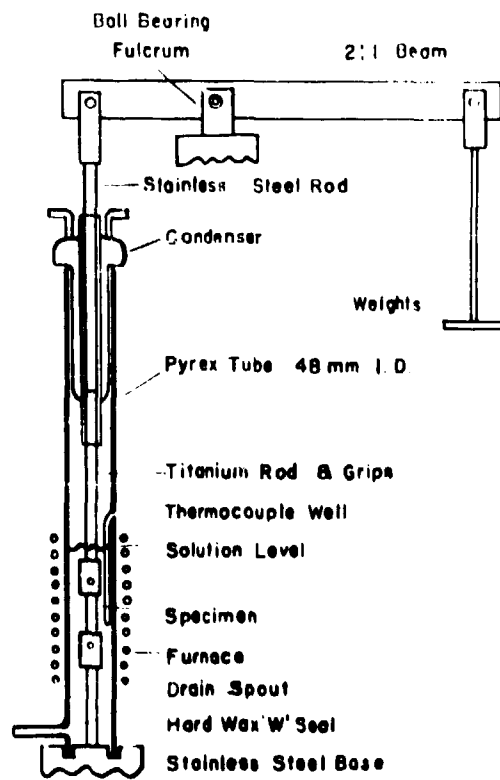


Figure 3. Schematic Drawing of Apparatus for Stress Corrosion Testing.



Figure 4. Crack at Pit in Fe-20Cr-20Ni Single Crystal 180x.



Figure 5. Cracks Occurring at Attack Slip Line on Fe-20Cr-20Ni Single Crystal 500x.



Figure 6. Cracks Nucleating on Surface of Recrystallized Area
in Fe-20Cr-20Ni 50x.

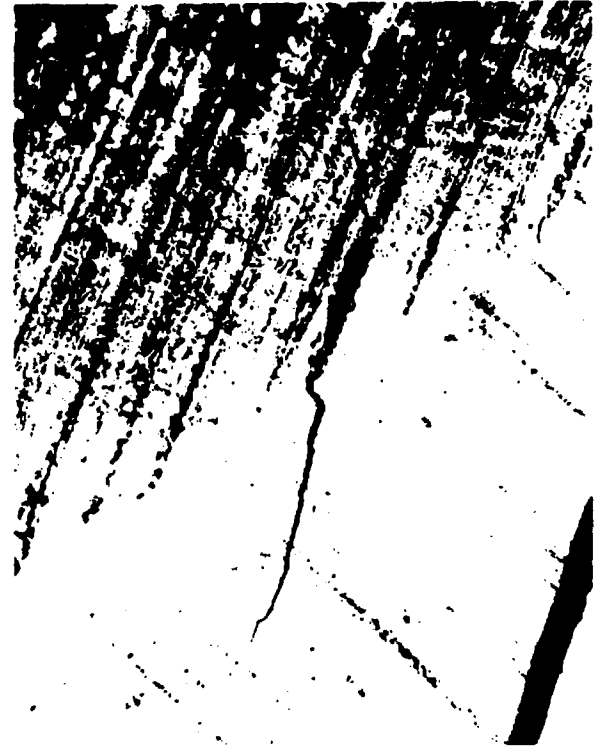


Figure 7. Close-up of Crack Nucleating Near Grain Boundary in
Fe-20Cr-20Ni 600x.



Figure 8. Crack in Recrystallized Area in Fe-20Cr-20Ni Specimen
160x.

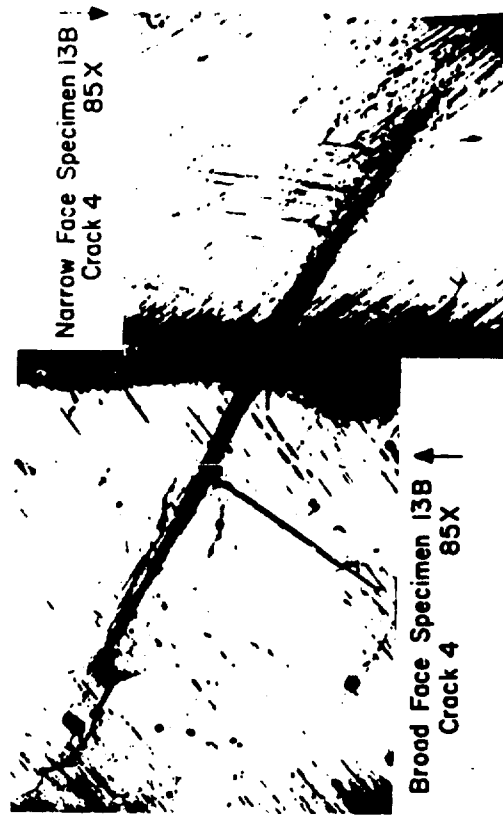


Figure 9. Composite Photomicrograph, Showing Typical Crack Trace as Seen on Two Surfaces in Fe-20Cr-20Ni Single Crystal 85x.

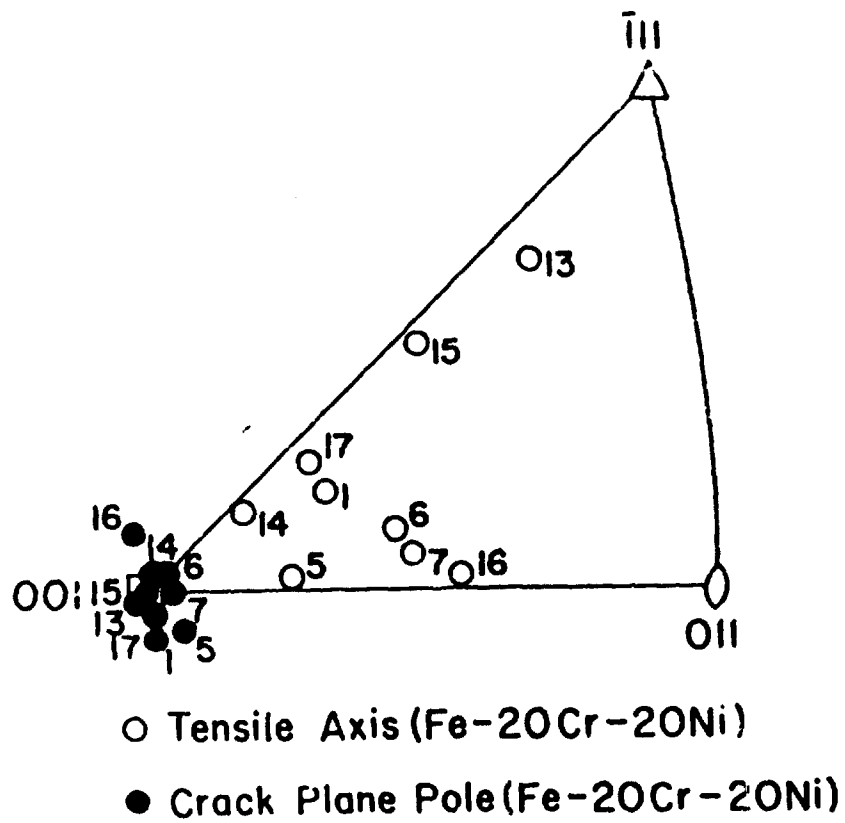


Figure 10. Unit Triangle Stereogram Showing Position of Crack Plane Poles and Tensile Axes for Fe-20Cr-20Ni Single Crystals.

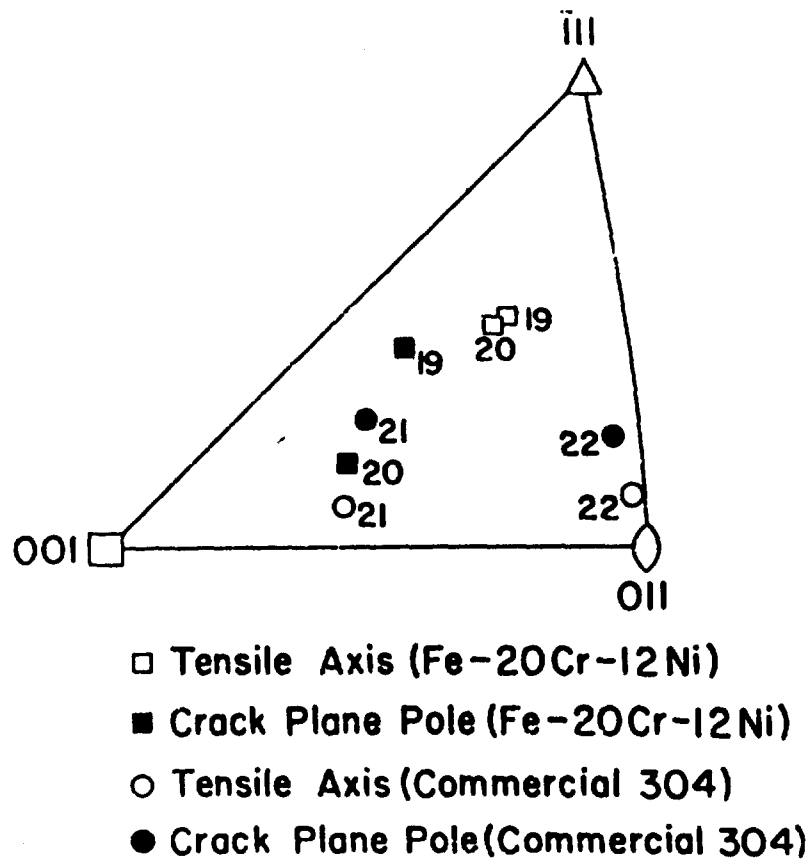


Figure 11. Unit Triangle Stereogram Showing Position of Crack Plane Poles and Tensile Axes for Commercial 304 and Fe-20Cr-12Ni Single Crystals.



Figure 12. Electron Micrograph Illustrating Cubic Block Structure of Fe-20Cr-20Ni Fracture Surface 7500x.

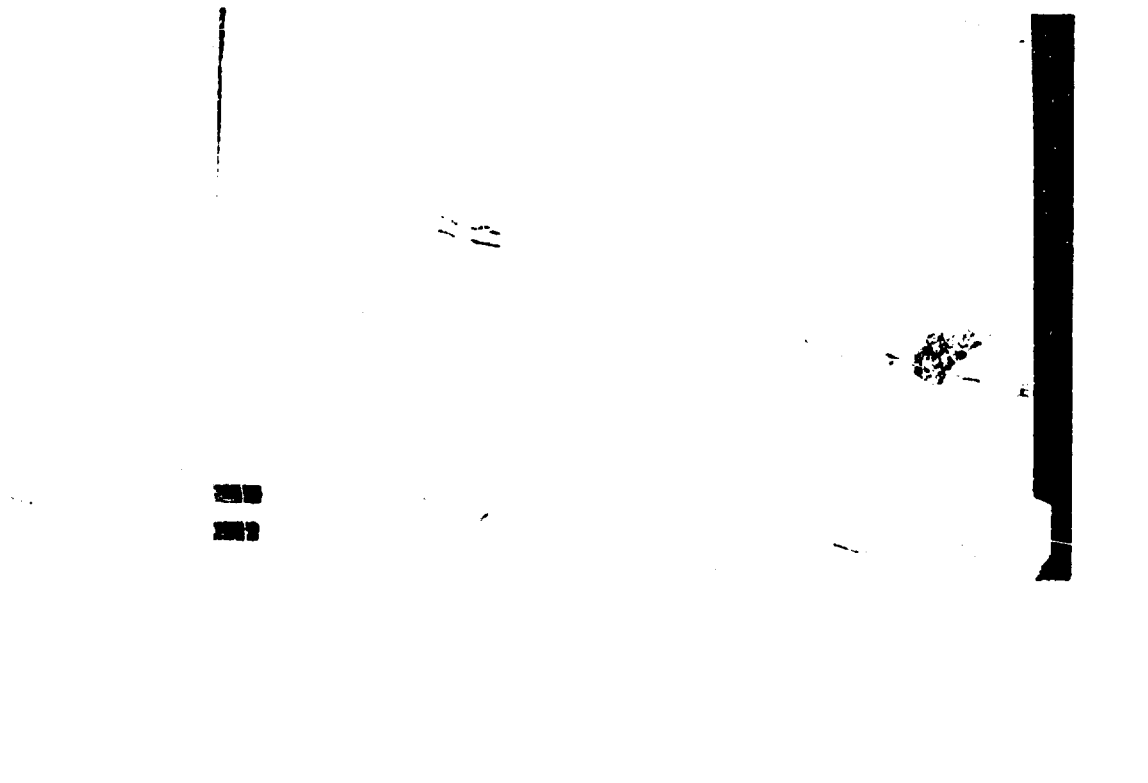
The image is a high-magnification electron micrograph of a fracture surface. It shows a complex, stepped topography with several distinct ledges and plateaus. Fine, parallel lines, characteristic of slip line traces, are visible on the surface. The image is framed by a dark border, and there are some dark, rectangular artifacts on the left and right sides, likely from the scanning process or the original print.

Figure 13. Electron Micrograph Showing Ledges with Step-wise Edges and Slip Line Traces on Fe-20Cr-20Ni Fracture Surface 7500x.



Figure 14. Electron Micrograph of Fracture Surface Structure on Commercial 304 Single Crystal 9500x.

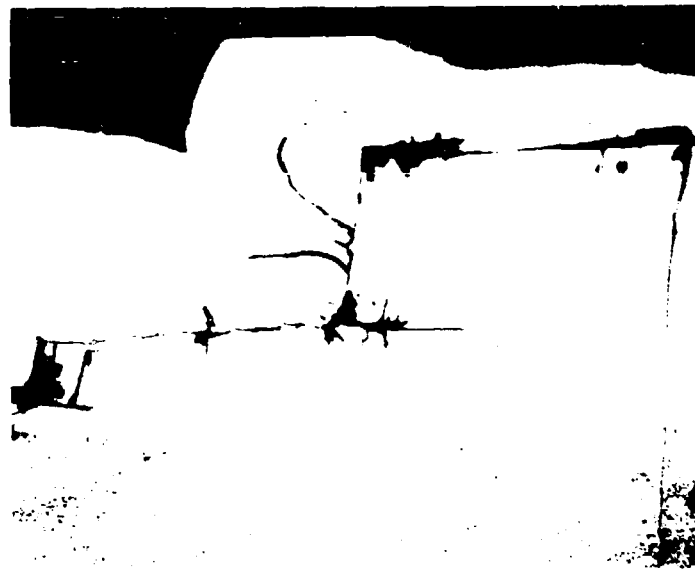


Figure 15. Section of Nickel Plated Fracture Surface Profile
of Fe-20Cr-20Ni 400x.